Acceptor-Donor-Acceptor small molecules based on derivatives of 3,4-ethylenedioxythiophene for solution processed organic solar cells

B. Y. Antwi,[a,b] R. G. D. Taylor,[b] J. Cameron,[b] R. B. Owoare,[a] R. Kingsford-Adaboh[a*] and P. J. Skabara[b*]

[a] Department of Chemistry, University of Ghana, Legon, Accra, Ghana.

[b] WestCHEM, Department of Pure and Applied Chemistry, University of Strathclyde, 295 Cathedral Street, Glasgow, G1 1XL, United Kingdom.

* Corresponding authors

Abstract

Three simple semiconducting acceptor-donor-acceptor (A-D-A) small molecules based on an electron-rich (3,4-ethylenedioxythiophene) EDOT central core have been synthesised (**DIN-2TE**, **DRH-2TE**, **DECA-2TE**) and characterised. Organic photovoltaic (OPV) devices incorporating these materials have been prepared and evaluated. The physical properties of the molecules were characterised by TGA, DSC, UV/vis spectroscopy and cyclic voltammetry. The HOMO-LUMO energy gaps of the molecules in the solid state were in the range 1.57 - 1.82 eV, and in solution 1.88 - 2.04 eV. Electrochemical HOMO-LUMO energy gaps determined by cyclic voltammetry were found to be in the range 1.97 - 2.31 eV. The addition of 1% diiodooctane (DIO) to photoactive blends of the A-D-A molecules and $PC_{71}BM$ more than doubled the power conversion efficiency (PCE) in the case of **DRH-2TE**:$PC_{71}BM$ devices to 1.36%.

Introduction

The use of organic materials as photoactive components in solar cells is of great interest[1] due to their flexibility, ease of processing, large area applicability, tunability and the availability of raw materials,[2–4] all of which are attributes that make them favourable compared to traditional silicon based devices. Recently, the use of small molecule, rather than polymeric, organic donors has gained attention due to their added advantages of well-defined molecular structure, low batch-to-batch variation[5,6] and high open circuit voltages (V_{oc}).[7] This has led to some impressively high PCEs for the top performing small molecule OPV devices (9.95%),[8] approaching the records of polymeric devices (11.5%).[1,9] However, many of these

top performing materials have complex structures with multi-step syntheses which result in a high cost and low overall yield. As Roncali *et al*.[10] recently remarked, *'small is beautiful'* and truly small, simple organic donor molecules that have a simplistic and scalable synthesis[5,11] should not be overlooked, even if their PCEs are lower than their more complex counterparts. Such materials are not only of interest as outright donors for OPV, but also as additives in ternary blend devices, which often exhibit enhanced PCE over their binary analogues.[12,13]

In an effort to tune the properties of organic donor materials, several *push-pull* type structures have been explored where the conjugated backbone consists of alternating donor (D) and acceptor (A) units. This is most prevalent in D/A copolymers,[14–16] but many small molecule architectures with D-A-D,[17–20] A-D-A,[21] D_1-A-D_2-A-D_1,[22] A'(D'AD)$_2$,[23] and D-A-D-π-D-A-D[24] motifs (where π represents a conjugated linker) have also been investigated. Of these, the A-D-A architecture is particularly attractive due to the high device performances achieved[8,25–27] and also because their synthesis is straightforward. In these molecules, alkyl cyanoacetate, rhodanine, indanedione and dicyanovinyl moieties[27–34] are found to be efficient electron-acceptor groups, whilst typical donor components are; thiophene, benzodithiophene, dithienosilole, silafluorene, fluorene and carbazole.[21] However, use of the strongly electron donating unit 3,4-ethylenedioxythiophene (EDOT) in A-D-A small molecule OPV devices has little precedent in the literature[10,35] even though it has been commonly studied in other small molecule D/A architectures[10,36,37] and polymeric devices.[38–42] The ability of EDOT to induce planarity through non-covalent O---S interactions with neighbouring donor units increases the backbone rigidity and effective conjugation, which in turn narrows the HOMO-LUMO energy gap.[43,44] This makes EDOT an attractive donor in the design of conjugated A-D-A small molecules for OPVs.

Herein, we report the first examples of A-D-A small molecules designed to utilise the planarising effect of EDOT in combination with acceptor units 1,3-indanedione, 3-ethylrhodanine and ethyl cyanoacetate. The

molecules were synthesised through a simple synthetic strategy utilising C-H activation to couple EDOT to 5-bromo-4-hexylthiophene-2-carbaldehyde to give **2TE**, which then underwent subsequent Knoevenagel condensations with methylene containing acceptor units (Scheme 1). The resultant materials (**DIN-2TE**, **DRH-2TE** and **DECA-2TE**) showed good potential as electron donors, with LUMO energy levels suitable to work with that of $PC_{71}BM$ (-4.13 eV)[45] for efficient exciton dissociation and charge transport. The device performances were optimised by varying the D/A weight ratio, applying various thermal annealing temperatures and changing the volume ratio of DIO additive.

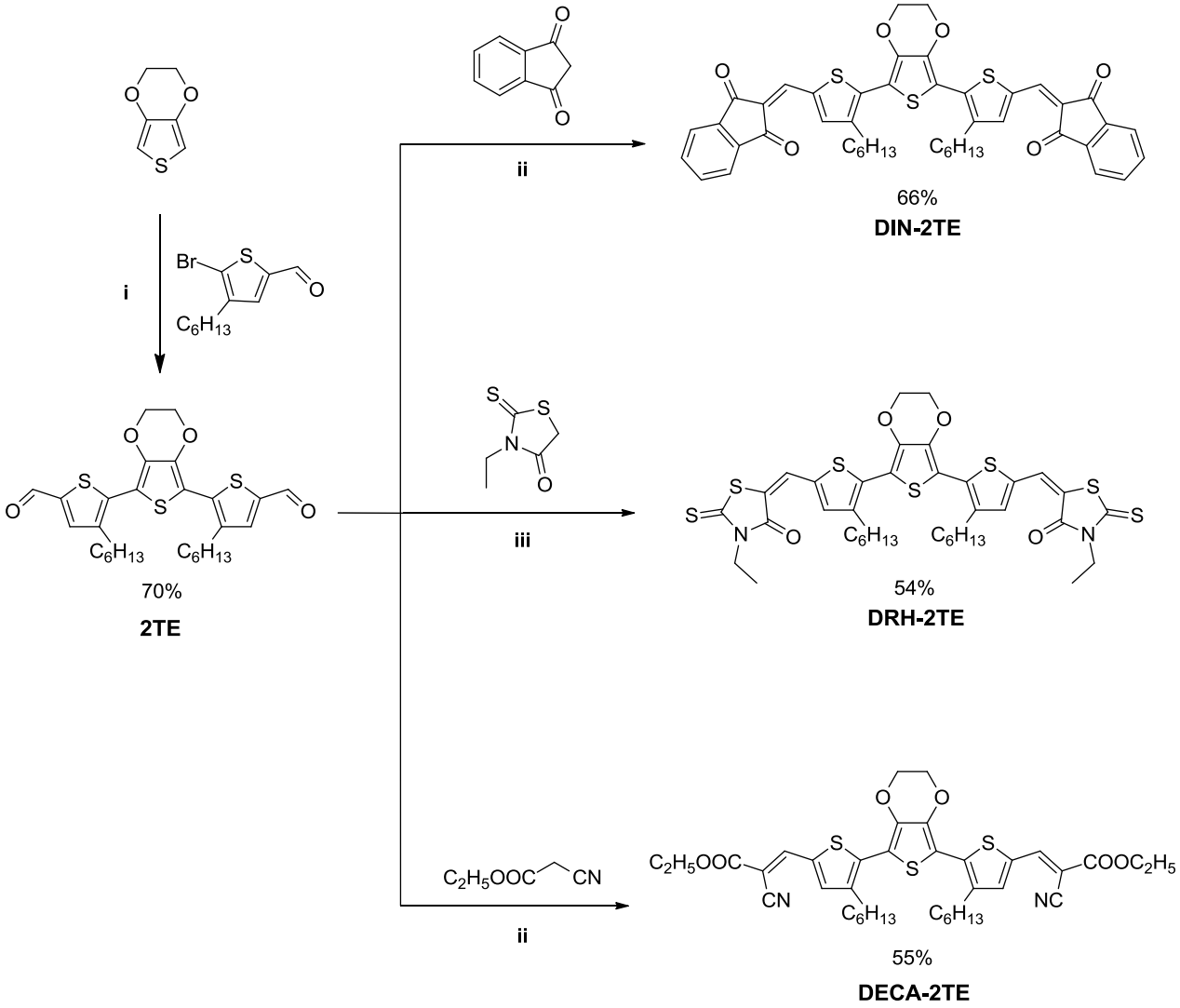

Scheme 1 *Reagents and conditions*: (i) Cs_2CO_3, pivalic acid, $Pd(OAc)_2$, $PCy_3{\cdot}HBF_4$, DMF, 110°C 16 h; (ii) NEt_3, $CHCl_3$, reflux, 16 h; (iii) piperidine, $CHCl_3$, reflux, 16 h.

Results and discussion

Thermal Properties

The thermal behaviour of **DIN-2TE**, **DRH-2TE** and **DECA-2TE** was explored by differential scanning calorimetry (DSC) and thermogravimetric analysis (TGA). The melting points determined by DSC of **DECA-2TE, DRH-2TE** and **DIN-2TE** were 236°C, 249°C and 335°C, respectively (detailed plots in SI)**.** TGA analysis (Figure 1) shows that thll molecules have good thermal stability with 5% weight loss temperatures (T_d) all above 350°C (Table 1).

Table 1. Electrochemical, thermal and optical characteristics of **DIN-2TE**, **DRH-2TE** and **DECA-2TE**.

Compound	Optical measurements					Electrochemical measurements			T_d (°C)
	Solution			Film					
	λ_{max} (nm)	E_{gap} (eV)[a]	ε (L mol^{-1} cm^{-1})	λ_{max} (nm)	E_{gap} (eV)[a]	HOMO (eV)[b]	LUMO (eV)[b]	E_g (eV)[c]	
DIN-2TE	570	1.88	7.3 ×10^4	592	1.57	-5.49	-3.18	2.31	360
DRH-2TE	545	1.93	5.2×10^4	550	1.71	-5.13	-3.16	1.97	362
DECA-2TE	510	2.08	4.0 ×10^5	513	1.82	-5.46	-3.30	2.16	363

[a]Solution and solid state optical HOMO-LUMO gaps were calculated from the onset of the longest wavelength absorption peak using $E = hc/\lambda$ and converting to eV. [b]HOMO and LUMO levels were calculated in reference to the Fc/Fc^+ redox couple; $E^{HOMO(LUMO)} = (-4.80 - E_{onset}^{ox(red)})$. [c]Electrochemical HOMO-LUMO gap = $E^{HOMO} - E^{LUMO}$.

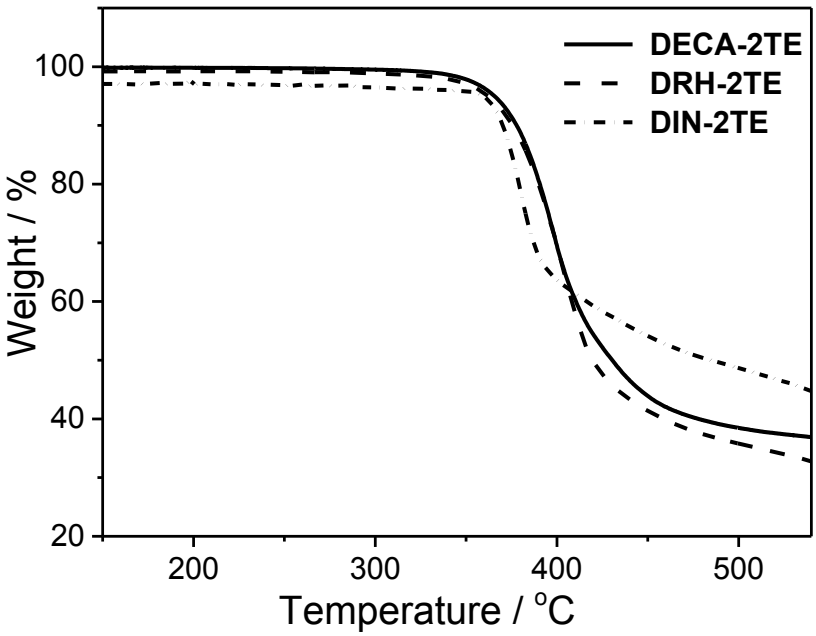

Figure 1. TGA plots of **DIN-2TE**, **DR-2TE** and **DECA-2TE** measured at 10°C min^{-1} under argon.

Optical and electrochemical properties.

All three A-D-A molecules showed strong absorption from 400 – 600 nm, extending up to 700 nm for **DIN-2TE**, arising from electronic π-π* transitions resulting in narrow HOMO-LUMO energy gaps (Table 1). **DIN-2TE**, **DRH-2TE** and **DECA-2TE** showed a λ_{max} of 570 nm, 545 nm and 510 nm, respectively. **DECA-2TE** showed the strongest absorption in the visible region with an extinction coefficient of 4.0×10^5 L mol^{-1} cm^{-1}. Broader absorption peaks observed in the solid state spectra, compared to the solution state spectra (Figure 2b), led to a red-shifted absorbance which may be due to strong aggregation as well as rigid and planar backbones of the molecules in the solid state. This is in agreement with previous studies of molecules containing the same acceptor group.[45] The optical HOMO-LUMO energy gaps, estimated from the lowest energy onset of the longest wavelength absorption band in both solution and thin film, are outlined in Table 1. The HOMO-LUMO energy gaps for all compounds narrowed in the solid state compared to solution. **DIN-2TE** showed the lowest energy gap (1.57 eV) in the solid state, followed by **DRH-2TE** (1.71 eV) and **DECA-2TE** (1.82 eV).

Cyclic voltammograms of **DIN-2TE**, **DRH-2TE** and **DECA-2TE** are shown in Figure 3. **DIN-2TE** showed two irreversible oxidation waves and one irreversible reduction wave with potentials at +0.69 V, +1.16 V and -

1.62 V, respectively. **DRH-2TE** showed two reversible oxidation processes at half-wave potentials of +0.33 V and +0.72 V, as well as an irreversible oxidation and reduction at +1.14 V and -1.64 V. Two reversible oxidation waves and one quasi-reversible reduction wave were found for **DECA-2TE** at half-wave potentials of +0.66 V, +1.15 V and -1.50 V respectively. We attribute the oxidation potentials to the electron-rich EDOT central donor and the reduction potentials to the electron deficient acceptor units. Therefore, an increasing order of acceptor electron withdrawing strength shows DECA (-1.50 V) > DIN (-1.62 V) > DRH (-1.64 V), resulting in LUMO energy levels of -3.30, -3.18 and -3.16 eV for **DECA-2TE**, **DIN-2TE** and **DRH-2TE** respectively (Table 1). The HOMO energy levels of **DECA-2TE** and **DIN-2TE** show little variation (-5.49 and -5.46 eV respectively), however a shallower HOMO energy level of **DRH-2TE** (-5.13 eV) results in a narrower HOMO-LUMO energy gap of (1.97 eV) compared to **DECA-2TE** and **DIN-2TE** (2.16 and 2.31 eV respectively).

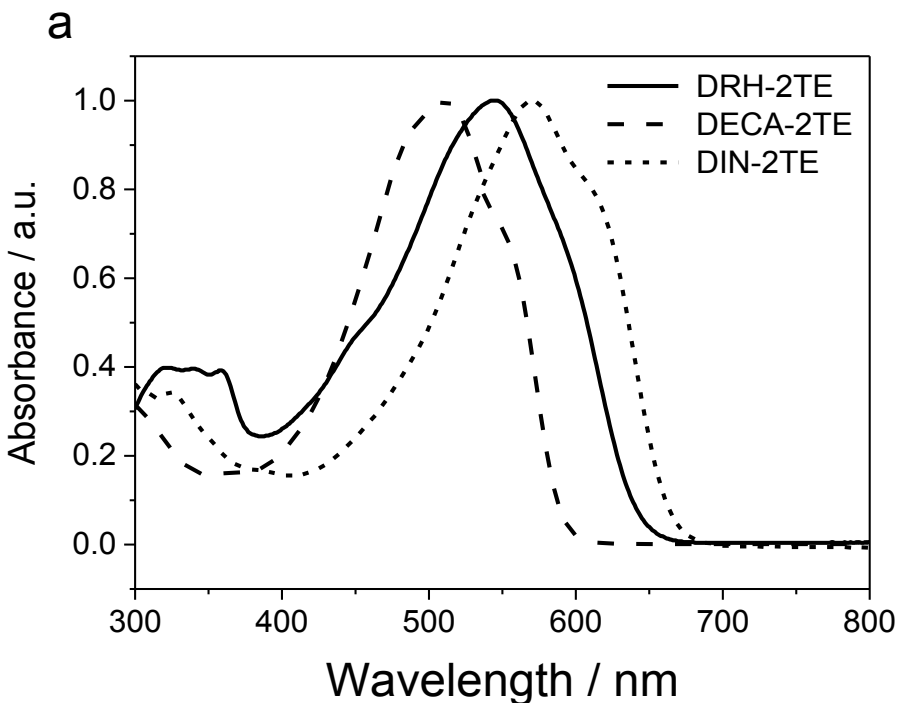

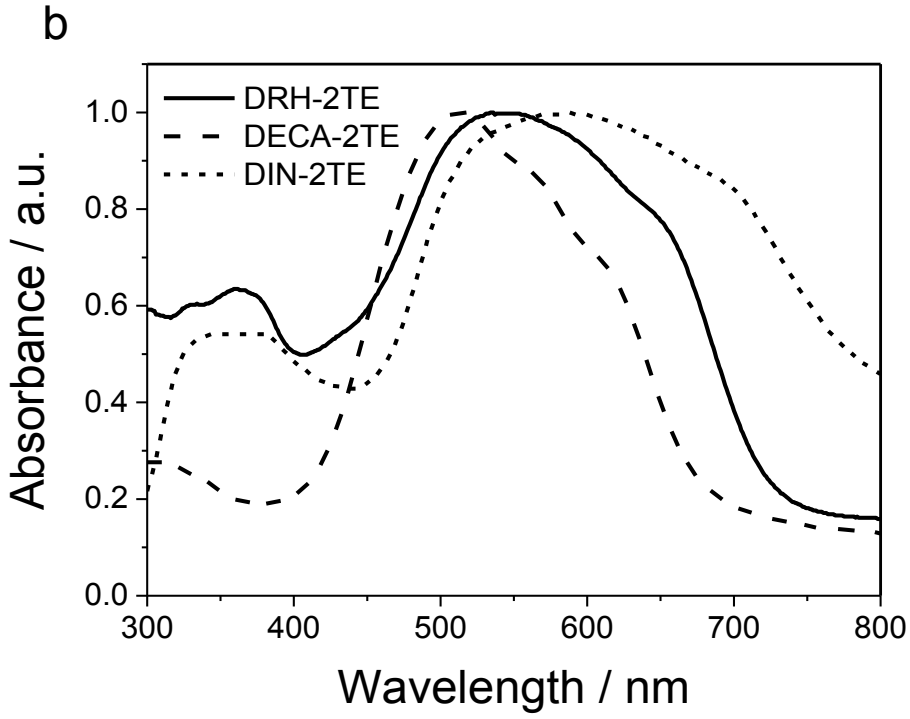

Figure 2 Normalised absorption spectra of **DIN-2TE**, **DRH-2TE**, and **DECA-2TE** (a) in chloroform solution (10^{-5} M) and (b) drop cast film on quartz glass.

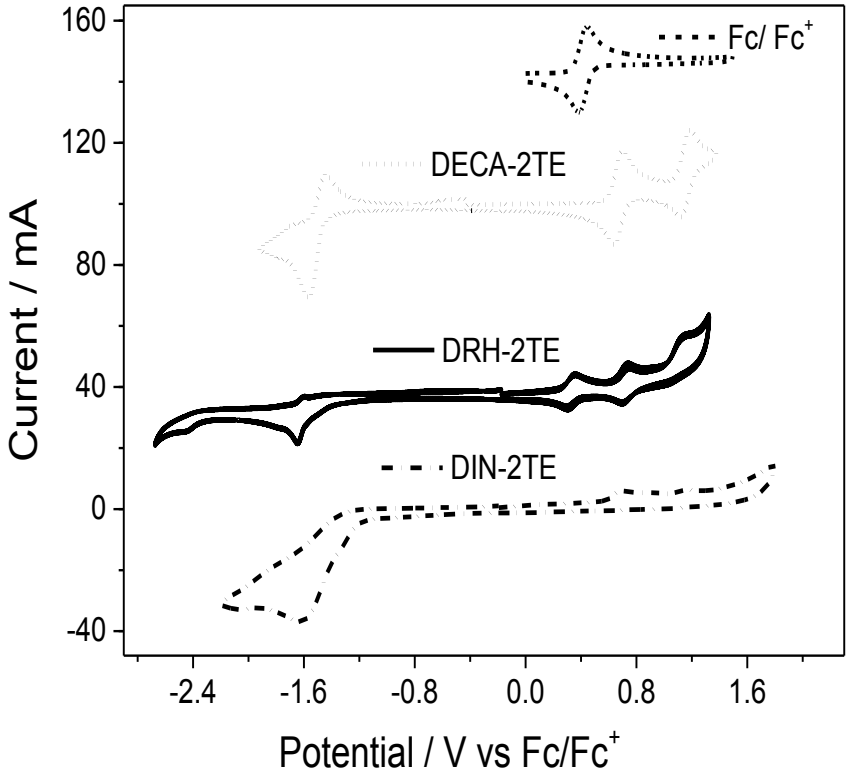

Figure 3 Cyclic voltammograms of **DIN-2TE**, **DRH-2TE**, and **DECA-2TE** in dichloromethane solution (10^{-4} M) with Bu_4NPF_6 as the supporting electrolyte (0.1 M). Recorded at a scan rate of 100 mV s^{-1} using platinum wire (counter), silver wire (reference) and glassy carbon (working) electrodes.

Organic photovoltaic devices

OPV device performances of the A-D-A small molecules were investigated using the bulk-heterojunction architecture with indium tin oxide (ITO) and calcium as the electrodes and poly(3,4-ethylenedioxythiophene):polystyrene sulfonate (PEDOT:PSS) as a hole transport layer, with a device structure of glass/ITO/PEDOT:PSS/photoactive layer/Ca (40 nm)/Al (40 nm) (Figure 4). The photoactive layer was processed from a chloroform solution of each small molecule donor and [6,6]-phenyl C_{71} butyric acid methyl ester ($PC_{71}BM$) acceptor. However, unexpected limited solubility of **DIN-2TE** led to poor film formation, such that devices fabricated using this donor gave no electrical response. The greater solubility of **DRH-2TE** and **DECA-2TE** allowed for device fabrication and the study of varying donor/acceptor (D/A) weight ratios, annealing temperatures and the use of 1,8-diiodooctane (DIO) as an additive for **DRH-2TE**:$PC_{71}BM$ and **DECA-2TE**:$PC_{71}BM$ devices. The use of DIO in OPV devices often leads to an increased performance which has been attributed to the selective solubilising of the fullerene acceptor in the DIO. This improves intermixing between the donor and acceptor causing the formation of long, narrow donor rich and acceptor rich domains, which subsequently leads to an improved short circuit current (J_{SC}).[46,47] Averaged optimised device performances are shown in Table 2.

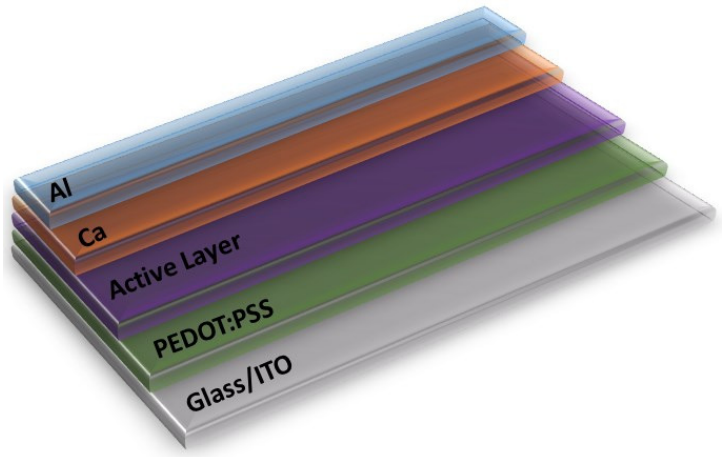

Figure 4 Structure of OPV devices fabricated. Ca/Al layer thickness 40 nm.

DRH-2TE:$PC_{71}BM$ devices at an optimum D/A weight ratio (1:3) and annealing temperature (90°C) gave a power conversion efficiency (PCE) of 0.63%, with an open circuit voltage (V_{oc}) of 0.64 V, low fill factor (FF) (0.30) and J_{sc} of 3.04 mA cm^{-2}. Optimised **DECA-2TE**:$PC_{71}BM$ devices demonstrated a better PCE of 1.03% at a D/A weight ratio of 1:4 and annealing temperature of 60°C, attributable to a superior V_{oc} (0.85 V) and FF (0.41), compared to **DRH-2TE**:$PC_{71}BM$ devices. Diverse PCEs of A-D-A small molecules can be accredited to the differing V_{oc} values which are related to the difference between the donor HOMO and acceptor LUMO energy levels.[45] Therefore, the deep HOMO level (-5.46 eV) of **DECA-2TE** resulted in a higher V_{oc} (0.85 V) in comparison to the shallower HOMO level of **DRH-2TE** (-5.13 eV) and lower V_{oc} (0.64 V). The LUMO level of the donor molecules also contributed to varied device performance, consistent with predictions made by Scharber *et al*..[48] Therefore, a donor with an improved V_{oc} due to a deeper HOMO energy level, combined with a LUMO energy level close to that of $PC_{71}BM$ (for efficient charge separation), will lead to higher J_{sc} and enhanced PCE.

Accordingly, attempts to improve J_{sc} by optimising device morphology were pursued through the use of DIO as an additive in the D/A blend at different volume ratios. As shown in Table 2, the efficiency of both **DRH-2TE**:$PC_{71}BM$ and **DECA-2TE**:$PC_{71}BM$ devices improved through the addition of 1% DIO. Other ratios of DIO were tested (see SI), but did not improve performance. PCEs of **DECA-2TE**:$PC_{71}BM$ (1:4 weight ratio)

devices increased slightly from 1.03% to 1.05%, but **DRH-2TE**:$PC_{71}BM$ (1:3 weight ratio) PCEs more than doubled (0.63% to 1.36%). This can be attributed to a large improvement in J_{sc} (3.04 vs 5.60 mA cm^{-2}). Figure 5 shows the *J-V* curves of A-D-A small molecule:$PC_{71}BM$ devices with and without 1% DIO.

Table 2. Summary of the average optimised photovoltaic performance for **DRH-2TE** and **DECA-2TE** devices. AM 1.5G illumination.

Photoactive blend (weight ratio)	J_{sc} (mA cm^{-2})	V_{oc} (V)	FF	PCE (%)
DRH-2TE: $PC_{71}BM$ (1:3) [a]	3.04	0.64	0.30	0.63
DRH-2TE: $PC_{71}BM$ (1:3) [a c]	5.60	0.68	0.35	1.36
DECA-2TE: $PC_{71}BM$ (1:4) [b]	2.96	0.85	0.41	1.03
DECA-2TE: $PC_{71}BM$ (1:4) [b c]	2.99	0.90	0.39	1.05

[a]60°C and [b]90°C annealing temperatures for 20 mins, [c]1 % diiodooctane.

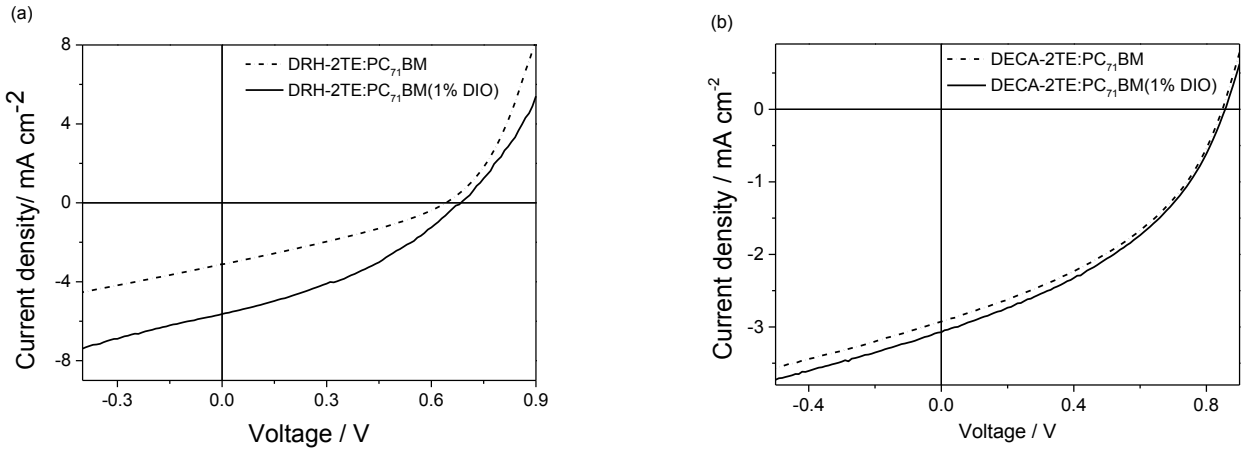

Figure 5. Current–voltage curves of optimised (a) **DRH-2TE**:$PC_{71}BM$ and (b) **DECA-2TE**:$PC_{71}BM$ bulk-heterojunction devices without and with 1% DIO additive under AM 1.5 G illumination.

Morphological Study

Atomic force microscopy (AFM) was used to investigate the morphology of the enhanced device performance for optimised **DRH-2TE**:$PC_{71}BM$ (1:3) (90°C) and **DECA-2TE**:$PC_{71}BM$ (1:4) (60°C) devices, with and without 1% DIO as shown in Figures 6 and 7, respectively.

Devices containing **DRH-2TE**:$PC_{71}BM$ (1:3) showed a smoother surface morphology (RMS roughness 18.3 nm) with 1% DIO compared to those without (RMS roughness = 44.9 nm) (Figure 6), indicating reduced D/A domain sizes giving rise to a more uniform film and improved device performance.[49] Accordingly, the smaller domains of interpenetrating D/A aggregates in the **DRH-2TE**:$PC_{71}BM$ devices with 1% DIO (compared to the larger aggregates in devices without DIO, Figure 6) resulted in enhanced charge separation, leading to an improved J_{sc} (3.04 *vs* 5.60 mA cm^{-2}) and PCE (0.63 *vs* 1.36%).

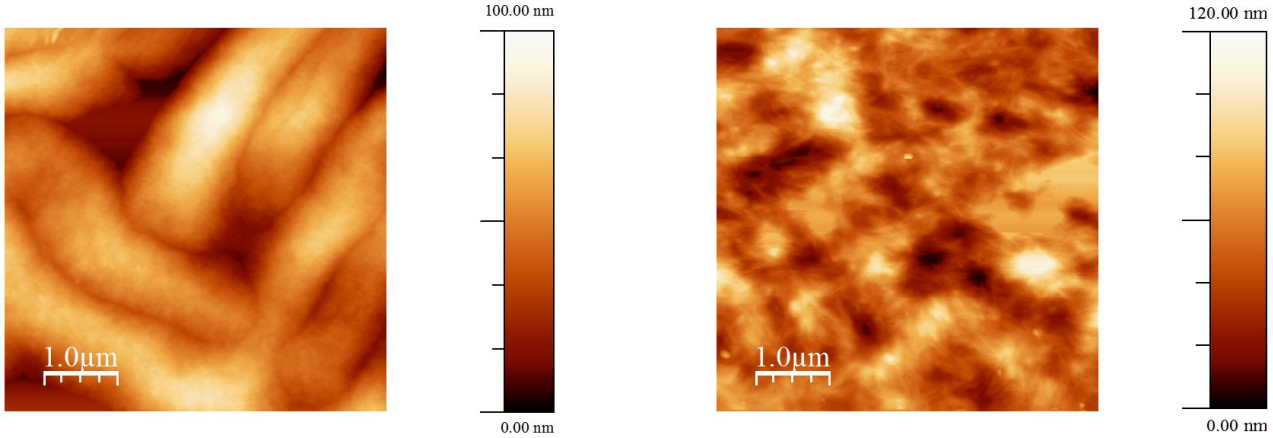

Figure 6: Tapping mode AFM height images of the best performing **DRH-2TE**:$PC_{71}BM$ device without DIO (left) and with 1% DIO (right). 1:3 D/A weight ratio, annealed at 90°C.

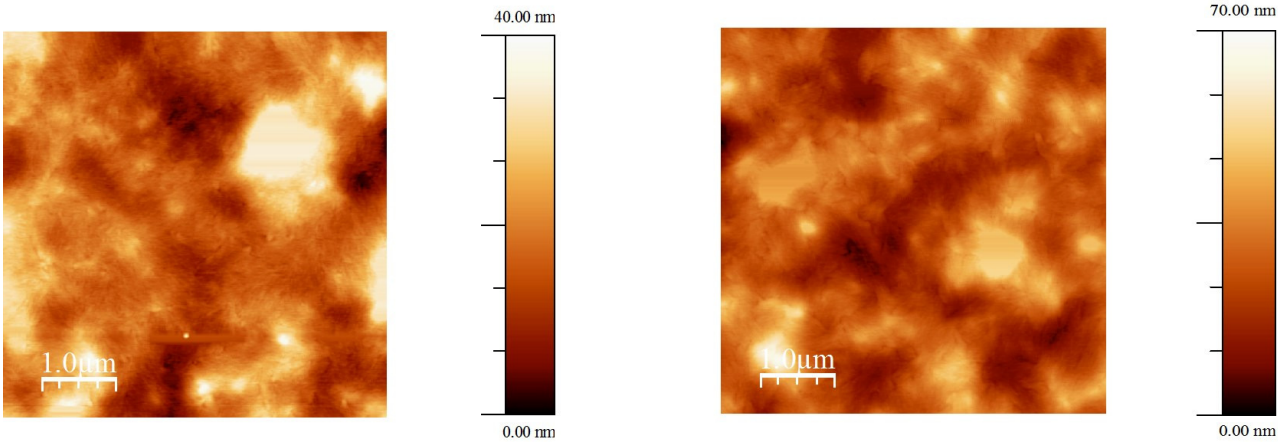

Figure 7: Tapping mode AFM height images of the best performing **DECA-2TE**:$PC_{71}BM$ device without DIO (left) and with 1% DIO (right). 1:4 D/A weight ratio, annealed at 60°C.

In contrast, the surface morphologies of **DECA-2TE** with and without 1% DIO look similar (Figure 7), suggesting that the DIO did not have any significant effect on the micromorphology, and thus gave no significant improvement in J_{SC} or PCE. Figure 7 shows that narrow fibre-like domains which are favourable for charge transport are already present without the addition of DIO, demonstrating that **DECA-2TE**/$PC_{71}BM$ blends have the ability to aggregate into optimal domain sizes without the need of an additive or co-solvent. This effect has been reported previously[50] and attributed to strong aggregation of the donor, resulting in no morphological change through DIO addition. Given that DIO has been shown to cause decreased photostability in the active layer of OPV devices,[51] there is an advantage in using donor materials such as **DECA-2TE**, which do not require use of a co-solvent to form a suitable morphology.

Summary

Three simple, low HOMO-LUMO energy gap semiconducting A-D-A small molecule donors (**DIN-2TE**, **DRH-2TE** and **DECA-2TE**) have been synthesised and fully characterised. **DIN-2TE** demonstrated the lowest optical HOMO-LUMO energy gap in both solution and solid state (1.88 and 1.57 eV, respectively). A shallower HOMO (-5.13 eV) of **DRH-2TE** contributed to a narrower electrochemical HOMO-LUMO energy gap (1.97 eV) compared to **DIN-2TE** (2.31 eV) and **DECA-2TE** (2.16 eV). Working OPV devices were realised for **DRH-2TE**:$PC_{71}BM$ and **DECA-2TE**:$PC_{71}BM$, with PCEs for **DRH-2TE**-based devices more than doubling with the addition of 1% DIO (0.63 vs 1.36%). Devices containing **DECA-2TE** showed very little improvement with the addition of 1% DIO, which can be attributed to the optimal film morphology achieved without the addition of DIO. These results demonstrate that the choice of acceptor unit in A-D-A type molecules has an impact on more than just the optical and electrochemical properties of the resultant material. As such, careful consideration of aggregation, solubility and the use of additives should be employed when designing such materials and their device structures.

Acknowledgements

PJS thanks the Royal Society for a Wolfson Research Merit Award. BYA is grateful for a Leverhulme-Royal Society Africa Award and a University of Ghana-Carnegie Next Generation of Academics Award. RGDT thanks the EPSRC for funding (EP/L012200/1). Supporting data are accessible from http://dx.doi.org/10.15129/baac5af3-4d02-4c1d-80ff-99e8eb42ce85.

References

1 National Renewable Energy Laboratory, *http://www.nrel.gov/ncpv/images/efficiency_chart.jpg*, 2016.

2 R. Po and J. Roncali, *J. Mater. Chem. C*, 2016, **4**, 3677–3685.

3 M. Shaker, J.-H. Lee, C. K. Trinh, W. Kim, K. Lee and J.-S. Lee, *RSC Adv.*, 2015, **5**, 66005–66012.

4 Q. An, F. Zhang, J. Zhang and W. Tang, *Energy Environ. Sci.*, 2016, **9**, 281–322.

5 H. Qin, L. Li, F. Guo, S. Su, J. Peng, Y. Cao and X. Peng, *Energy Environ. Sci.*, 2014, **7**, 1397.

6 G. D. Sharma, J. A. Mikroyannidis, R. Kurchania and K. R. J. Thomas, *J. Mater. Chem.*, 2012, **22**, 13986.

7 B. Walker, C. Kim and T. Q. Nguyen, *Chem. Mater.*, 2011, **23**, 470–482.

8 Q. Zhang, B. Kan, F. Liu, G. Long, X. Wan, X. Chen, Y. Zuo, W. Ni, H. Zhang, M. Li, Z. Hu, F. Huang, Y. Cao, Z. Liang, M. Zhang, T. P. Russell and Y. Chen, *Nat. Photonics*, 2014, **9**, 35–41.

9 J. Zhao, Y. Li, G. Yang, K. Jiang, H. Lin, H. Ade, W. Ma and H. Yan, *Nat. Energy*, 2016, **1**, 15027.

10 J. Roncali, P. Leriche and P. Blanchard, *Adv. Mater.*, 2014, **26**, 3821–3838.

11 D. Demeter, S. Mohamed, A. Diac, I. Grosu and J. Roncali, *ChemSusChem*, 2014, **7**, 1046–50.

12 L. Ye, H. Xu, H. Yu, W. Xu, H. Li, H. Wang, N. Zhao and J. Xu, *J. Phys. Chem. C*, 2014, **118**, 20094–20099.

13 P. Cheng and X. Zhan, *Mater. Horizons*, 2015, **2**, 462–485.

14 W. Li, L. Yang, J. R. Tumbleston, L. Yan, H. Ade and W. You, *Adv. Mater.*, 2014, 4456–4462.

15 J. W. Jung, J. W. Jo, E. H. Jung and W. H. Jo, *Org. Electron.*, 2016, **31**, 149–170.

16 Z. Zhang and J. Wang, *J. Mater. Chem.*, 2012, **22**, 4178.

17 D. Deng, Y. Yang, J. Zhang, C. He, M. Zhang, Z. G. Zhang, Z. Zhang and Y. Li, *Org. Electron.*, 2011, **12**, 614–622.

18 A. Yassin, P. Leriche, M. Allain and J. Roncali, *New J. Chem.*, 2013, **37**, 502–507.

19 J. Zhang, C. He, Z. Zhang and D. Deng, *Phil. Trans. R. Soc. A*, 2014, **372**, 20130009.

20 A. M. Coclite, R. M. Howden, D. C. Borrelli, C. D. Petruczok, R. Yang, J. L. Yagüe, A. Ugur, N. Chen, S. Lee, W. J. Jo, A. Liu, X. Wang and K. K. Gleason, *Adv. Mater.*, 2013, **25**, 5392–423.

21 W. Ni, X. Wan, M. Li, Y. Wang, Y. Chen and W. Ni, *Chem. Commun.*, 2015, **51**, 4936–4950.

22 C. V. Kumar, L. Cabau, E. N. Koukaras, G. D. Sharma and E. Palomares, *Org. Electron.*, 2015, **26**, 36–47.

23 M. Shaker, J. Lee, C. K. Trinh, W. Kim, K. Lee and J. Lee, *RSC Adv.*, 2015, **5**, 66005–66012.

24 Y. Patil, R. Misra, A. Sharma and G. D. Sharma, *Phys. Chem. Chem. Phys.*, 2016, **18**, 16950–16957.

25 J. Zhou, Y. Zuo, X. Wan, G. Long, Q. Zhang, W. Ni, Y. Liu, Z. Li, G. He, C. Li, B. Kan, M. Li and Y. Chen, *J. Am. Chem. Soc.*, 2013, **135**, 8484–8487.

26 M. Cheng, C. Chen, X. Yang, J. Huang, F. Zhang, B. Xu and L. Sun, *Chem. Mater.*, 2015, **27**, 1808–1814.

27 G. He, Z. Li, X. Wan, J. Zhou, G. Long, S. Zhang, M. Zhang and Y. Chen, *J. Mater. Chem. A*, 2013, **1**, 1801–1809.

28 G. He, X. Wan, Z. Li, Q. Zhang, G. Long, Y. Liu, Y. Hou, M. Zhang and Y. Chen, *J. Mater. Chem. C*, 2014, **2**, 1337–1345.

29 Y. Zhou, M. Xiao, D. Liu, Z. Du, W. Chen, D. Ouyang, L. Han, X. Wan and R. Yang, *Org. Electron.*, 2015, **17**, 355–363.

30 Y. Kim, C. E. Song, S. Moon, E. Lim, V. A. Online, Y. Kim, C. E. Song, S. Moon and E. Lim, *Chem. Commun.*, 2014, **50**, 8235–8238.

31 R. Fitzner, E. Reinold, A. Mishra, E. Mena-Osteritz, P. Bäuerle, H. Ziehlke, C. Körner, K. Leo, M. Riede, M. Weil, O. Tsaryova, A. Weiß, C. Uhrich and M. Pfeiffer, *Adv. Funct. Mater.*, 2011, **21**, 897–910.

32 Z. Wang, Z. Li, J. Liu, J. Mei, K. Li, Y. Li and Q. Peng, *ACS Appl. Mater. Interfaces*, 2016, **8**, 11639–11648.

33 Y. Lin, P. Cheng, Y. Liu, Q. Shi, W. Hu, Y. Li and X. Zhan, *Org. Electron.*, 2012, **13**, 673–680.

34 B. Kan, Q. Zhang, M. Li, X. Wan, W. Ni, G. Long, Y. Wang, X. Yang, H. Feng and Y. Chen, *J. Am. Chem. Soc.*, 2014, **136**, 15529–15532.

35 S. M. Tuladhar, M. Azzouzi, F. Delval, J. Yao, A. A. Y. Guilbert, T. Kirchartz, N. F. Montcada, R.

Dominguez, F. Langa, E. Palomares and J. Nelson, *ACS Energy Lett.*, 2016, **1**, 302–308.

36 D. Demeter, T. Rousseau and J. Roncali, *RSC Adv.*, 2013, **3**, 704.

37 A. Diac, D. Demeter, M. Allain, I. Grosu and J. Roncali, *Chem. Eur. J.*, 2015, **21**, 1598–1608.

38 C. Wang, C. J. Mueller, E. Gann, A. C. Y. Liu, M. Thelakkat and C. R. McNeill, *J. Mater. Chem. A*, 2016, **4**, 3477–3486.

39 J. Roncali, P. Blanchard and P. Frere, *J. Mater. Chem.*, 2005, **15**, 1589–1610.

40 N. I. Abdo, J. Ku, A. A. El-Shehawy, H.-S. Shim, J.-K. Min, A. A. El-Barbary, Y. H. Jang and J.-S. Lee, *J. Mater. Chem. A*, 2013, **1**, 10306.

41 A. M. Österholm, J. F. Ponder, J. A. Kerszulis and J. R. Reynolds, *ACS Appl. Mater. Interfaces*, 2016, **8**, 13492–13498.

42 A. M. Österholm, D. E. Shen, A. L. Dyer and J. R. Reynolds, *ACS Appl. Mater. Interfaces*, 2013, **5**, 13432–13440.

43 G. Conboy, H. Spencer, E. Angioni, A. Kanibolotsky, N. J. Findlay, S. Coles, C. Wilson, M. Pitak, C. Risko, V. Coropceanu, J. Bredas and P. Skabara, *Mater. Horiz.*, 2016, **3**, 333.

44 H. Pang, P. J. Skabara, S. Gordeyev, J. J. W. Mcdouall, S. J. Coles and M. B. Hursthouse, *Chem. Mater.*, 2007, **19**, 301–307.

45 J. Sim, H. Lee, K. Song, S. Biswas, A. Sharma, G. D. Sharma and J. Ko, *J. Mater. Chem. C*, 2016, **4**, 3508–3516.

46 A. Zusan, B. Gieseking, M. Zerson, V. Dyakonov, R. Magerle and C. Deibel, *Sci. Rep.*, 2015, **5**, 8286.

47 G. J. Hedley, A. J. Ward, A. Alekseev, C. T. Howells, E. R. Martins, L. A. Serrano, G. Cooke, A. Ruseckas and I. D. W. Samuel, *Nat. Commun.*, 2013, **4**, 2867.

48 M. C. Scharber, D. Mühlbacher, M. Koppe, P. Denk, C. Waldauf, A. J. Heeger and C. J. Brabec, *Adv. Mater.*, 2006, **18**, 789–794.

49 Z. Wang, F. Zhang, L. Li, Q. An, J. Wang and J. Zhang, *Appl. Surf. Sci.*, 2014, **305**, 221–226.

50 M. Saito, I. Osaka, Y. Suzuki, K. Takimiya, T. Okabe, S. Ikeda and T. Asano, *Sci. Rep.*, 2015, **5**, 14202.

51 B. J. Tremolet De Villers, K. A. O'Hara, D. P. Ostrowski, P. H. Biddle, S. E. Shaheen, M. L. Chabinyc, D. C. Olson and N. Kopidakis, *Chem. Mater.*, 2016, **28**, 876–884.